Inorg. Chem. **2008**, *47*, 2347−2355

Effect of π-Conjugated Length of Bridging Ligand on the Optoelectronic Properties of Platinum(II) Dimers

Li-Li Shi, Yi Liao, Guo-Chun Yang, Zhong-Min Su,* and Shan-Shan Zhao

Institute of Functional Material Chemistry, Faculty of Chemistry, Northeast Normal University, Changchun, Jilin, 130024, China

Received April 13, 2007

We report a quantum-chemical study of the electronic and optical properties of several platinum(II) dimers, $[Pt(pip_2NCN)]_2(L)^{2+}$ (pip_2NCNH = 1,3-bis(piperidylmethyl)benzene, L represents the bridging ligands pyrazine, 4,4′-bipyridine, or *trans*-1,2-bis(4-pyridyl)ethylene). The theoretical calculations reveal that as the π-conjugated length of bridging ligand increases, the energies of HOMOs and LUMOs, bonding energy of $Pt-N_{bridge}$, and the largest absorption strength increase whereas the ionization potentials decrease. According to the inner reorganization energy and density of states, we presume the hole-transporting properties of these dimers is better than the electron-transporting, and their inner reorganization energies for hole transport are lower than that of 4,4′-bis(phenyl-m-tolylamino)biphenyl (TPD), a well-known hole-transporting material. These platinum(II) dimers, especially $[Pt(pip_2NCN)]_2(bpe)^{2+}$, hold promise for use as a new kind of third-order nonlinear optical material, owing to their large third-order polarizabilty value and high transparency. Moreover, the optoelectronic properties of these complexes are easy to tailor by modifying the peripheral and central ligands. These theoretical results are beneficial to the design of new functional materials with excellent optoelectronic properties.

1. Introduction

In the past decades, organic ligands such as pyrazine (pyz),[1] *trans*-1,2-bis(4-pyridyl)ethylene (bpe),[2] and 4,4′-bipyridine (bpy)[2c,e,3] have been widely employed as building blocks for supramolecular platinum complexes. These complexes are apt to self-assemble,[1d,2a–c,3e,f] and possess some useful optoelectronic properties.[2h,3g,4] Jude et al.[5] have reported their excellent work on this type of supramolecular platinum(II) dimers $[Pt(pip_2NCN)]_2(L)^{2+}$ (pip_2NCNH = 1,3-bis(piperidylmethyl)benzene, L represents the bridging ligand) bridged by the organic ligands (pyz, bpy, and bpe), revealing the great differences in the luminescent behaviors of complexes when the bridging ligand varies. Besides the luminescent properties, other characteristics such as energy gap, ionization potential (IP), electron affinity (EA), and

* To whom correspondence should be addressed. E-mail: zmsu@nenu.edu.cn.

(1) (a) Albinati, A.; Isaia, F.; Kaufmann, W.; Sorato, C.; Venanzi, L. M. *Inorg. Chem.* **1989**, *28*, 1112–1122. (b) Komeda, S.; Kalayda, G. V.; Lutz, M.; Spek, A. L.; Yamanaka, Y.; Sato, T.; Chikuma, M.; Reedijk, J. *J. Med. Chem.* **2003**, *46*, 1210–1219. (c) Kumazawa, K.; Biradha, K.; Kusukawa, T.; Okano, T.; Fujita, M. *Angew. Chem., Int. Ed.* **2003**, *42*, 3909–3913. (d) Schweiger, M.; Seidel, S. R.; Arif, A. M.; Stang, P. J. *Angew. Chem., Int. Ed.* **2001**, *40*, 3467–3469. (e) Lu, W.; Chan, M. C. W.; Cheung, K.-K.; Che, C.-M. *Organometallics* **2001**, *20*, 2477–2486.

(2) (a) Kryschenko, Y. K.; Seidel, S. R.; Arif, A. M.; Stang, P. J. *J. Am. Chem. Soc.* **2003**, *125*, 5193–5198. (b) Schweiger, M.; Seidel, S. R.; Arif, A. M.; Stang, P. J. *Inorg. Chem.* **2002**, *41*, 2556–2559. (c) Schalley, C. A.; Muller, T.; Linnartz, P.; Witt, M.; Schafer, M.; Lutzen, A. *Chem.-Eur. J.* **2002**, *8*, 3538–3551. (d) Chen, W.; Liu, X.; You, X. *Chem. Lett.* **2002**, *734*, 735. (e) Kuehl, C. J.; Arif, A. M.; Stang, P. J. *Org. Lett.* **2000**, *2*, 3727–3729. (f) Lowe, G.; Droz, A. S.; Vilaivan, T.; Weaver, G. W.; Park, J. J.; Pratt, J. M.; Tweedale, L.; Kelland, L. R. *J. Med. Chem.* **1999**, *42*, 3167–3174. (g) Lowe, G.; McCloskey, J. A.; Ni, J.; Valaivan, T. *Bioorg. Med. Chem.* **1996**, *4*, 1007–1013. (h) Sun, S.-S.; Anspach, J. A.; Lees, A. J. *Inorg. Chem.* **2002**, *41*, 1862–1869. (i) Kaim, W.; Schwederski, B.; Dogan, A.; Fiedler, J.; Kuehl, C. J.; Stang, P. J. *Inorg. Chem.* **2002**, *41*, 4025–4028.

(3) (a) Cafeo, G.; Lo Passo, C.; Scolaro, L. M.; Pernice, I.; Romeo, R. *Inorg. Chim. Acta* **1998**, *275*, 141–149. (b) Orita, A.; Jiang, L.; Nakano, T.; Ma, N.; Otera, J. *Chem. Commun.* **2002**, 1362–1363. (c) Fujita, M.; Ibukuro, F.; Yamaguchi, K.; Ogura, K. *J. Am. Chem. Soc.* **1995**, *117*, 4175–4176. (d) Pfennig, B. W.; Mordas, C. J.; McCloskey, A.; Lockard, J. V.; Salmon, P. M.; Cohen, J. L.; Watson, D. F.; Bocarsly, A. B. *Inorg. Chem.* **2002**, *41*, 4389–4395. (e) Stang, P. J.; Cao, D. H. *J. Am. Chem. Soc.* **1994**, *116*, 4981–4982. (f) Stang, P. J.; Cao, D. H.; Saito, S.; Arif, A. M. *J. Am. Chem. Soc.* **1995**, *117*, 6273–6283. (g) Pfennig, B. W.; Mordas, C. J.; McCloskey, A.; Lockard, J. V.; Salmon, P. M.; Cohen, J. L.; Watson, D. F.; Bocarsly, A. B. *Inorg. Chem.* **2002**, *41*, 4389–4395.

(4) Balashev, K. P.; Khanukaeva, O. R. *Russ. J. Gen. Chem.* **2001**, *71*, 1149–1150.

(5) (a) Jude, H.; Bauer, J. A. K.; Connick, W. B. *Inorg. Chem.* **2005**, *44*, 1211–1220. (b) Jude, H.; Bauer, J. A. K.; Connick, W. B. *Inorg. Chem.* **2004**, *43*, 725–733.

10.1021/ic7018154 CCC: $40.75
Published on Web 03/06/2008

migration of charge[6] must be considered when new electrical and optical materials are designed. Moreover, the influence of the π-conjugated length of bridging ligand on these properties is also very interesting and an important topic, which is scarcely mentioned in other reports.

Nowadays, quantum-chemical calculations have been proved useful for gaining insight into the optoelectronic properties of organometallic complexes.[7] With theoretical calculations, the nature of photoexcitation or photoluminescence and the mechanism of charge transfer can be well explained.[8] To design new multifunctional materials, it is necessary to understand thoroughly the relationship between the electronic structure and optoelectronic properties. Hence, the theoretical investigation of platinum(II) dimers with electronically tunable bridging ligands has attracted considerable attention.

In this work, we study the effect of the π-conjugated length of bridging ligand on the structural, electronic, linear and nonlinear optical properties, and the carrier mobility of this series of platinum(II) dimers. We find the modification of bridging ligands will allow the optoelectronic properties of platinum(II) dimers to be modulated at the molecular level.

2. Computation Methods

The ground states for each molecule were calculated using density functional theory (DFT).[9] All open-shell calculations were performed using unrestricted methods (UDFT), and spin contamination in the radical species can be neglected (=0.75 after annihilation). Recent studies show that DFT calculations are remarkably successful in calculating molecular orbital distributions for the interpretation of electrochemical and photochemical results for Ru(II)[10] and square planar Pt(II) complexes.[11] Becke's three-parameter hybrid method[12] using the Lee–Yang–Parr correlation functional[13] (denoted as B3LYP) was adopted here. Gradient optimizations were performed using the 3-21G* basis set[14] for N, C, and H atoms. Because of large numbers of electrons and the attempt to account for relativistic effects, the platinum atom was represented by the ECP60MWB relativistic effective core potential from the Stuttgart/Bonn group (18 valence electrons) and its associated (8s7p6d)/[6s5p3d] basis set.[15] The above basis set for all atoms is abbreviated as E60. Subsequently, frequency calculations were performed at the same theoretical level to confirm that our predicted molecular structures were in the stable states. Geometry optimizations of the lowest triplet excited states (T_1) were performed at the unrestricted B3LYP/E60 level.

On the basis of ground- and excited-state optimization, the time-dependent density functional theory (TD-DFT) approach[16] was applied to investigation of the excited-state electronic properties of platinum(II) dimers at the B3LYP/E60 level. The solvent effect was simulated using the polarizable continuum model (PCM) in which the solvent cavity is regarded as a union of interlocking atomic spheres. All calculations were performed with the Gaussian 03[17] software package.

3. Results and Discussion

3.1. Selection of Model Systems. To save computation time, we employed an amino group (NH_2) as a substitute for the piperidyl group. The real systems and their corresponding model systems **1**, **2**, and **3** are shown in Figure 1. Subsequently, the complex $[Pt(pip_2NCN)]_2(pyz)^{2+}$ was used as an example to test this rationality. First, $[Pt(pip_2NCN)]_2(pyz)^{2+}$ and its corresponding model system **1** were optimized using DFT B3LYP/E60. The calculation results are listed in Table 1. It was observed that the coordination bond lengths were almost identical. Second, the distribution of total and partial density-of-states (DOS) of $[Pt(pip_2NCN)]_2(pyz)^{2+}$ was calculated using the Aomix program[18] on the basis of the optimized ground-state

(6) (a) Fukuda, M.; Sawada, K.; Yoshino, K. *J. Polym. Sci., Part A* **1993**, *31*, 2465–2471. (b) Klaener, G.; Miller, R. D. *Macromolecules* **1998**, *31*, 2009. (c) Greczynski, G.; Fahlman, M.; Salaneck, W. R. *Chem. Phys. Lett.* **2000**, *321*, 379–384.

(7) (a) Koentjoro, O. F.; Rousseau, R.; Low, P. J. *Organometallics* **2001**, *20*, 4502–4509. (b) Makedonas, C.; Mitsopoulou, C. A.; Lahoz, F. J.; Balana, A. I. *Inorg. Chem.* **2003**, *42*, 8853–8865. (c) Batista, E. R.; Martin, R. I. *J. Phys. Chem. A* **2005**, *109*, 3128–3133. (d) Urtel, H.; Bikzhanova, G. A.; Grotjahn, D. B.; Hofmann, P. *Organometallics* **2001**, *20*, 3938–3949. (e) Iron, M. A.; Martin, J. M. L.; Van der Boom, M. E. *J. Am. Chem. Soc.* **2003**, *125*, 11702–11709.

(8) (a) Stoyanov, S. R.; Villegas, J. M.; Rillema, D. P. *Inorg. Chem.* **2003**, *42*, 7852–7860. (b) Boulet, P.; Chermett, H.; Daul, C.; Gilardoni, F.; Rogemond, F.; Weber, J.; Zuber, G. *J. Phys. Chem. A* **2001**, *105*, 885–894. (c) Li, J.; Djurovich, P. I.; Alleyne, B. D.; Yousufuddin, M.; Ho, N. N.; Thomas, J. C.; Peters, J. C.; Bau, R.; Thompson, M. E. *Inorg. Chem.* **2005**, *44*, 1713–1727.

(9) (a) Koch, W.; Holthausen, M. C. *A Chemist's Guide to Density Functional Theory*; Wiley-VCH: Weinheim, Germany, 2000. (b) Adamo, C.; di Matteo, B. V. *Adv. Quantum Chem.* **1999**, *36*, 4.

(10) Nguyen, K. A.; Kennel, J.; Pachter, R. *J. Chem. Phys.* **2002**, *117*, 7128–7136.

(11) Stoyanov, S. R.; Villegas, J. M.; Rillema, D. P. *Inorg. Chem.* **2003**, *42*, 7852–7860.

(12) Becke, A. D. *J. Chem. Phys.* **1993**, *98*, 5648–5652.

(13) (a) Lee, C.; Yang, W.; Parr, R. G. *Phys. Rev. B* **1988**, *37*, 785–789. (b) Miehlich, B.; Savin, A.; Stoll, H.; Preuss, H. *Chem. Phys. Lett.* **1989**, *157*, 200–206.

(14) (a) Bauernschmitt, R.; Ahlrichs, R. *Chem. Phys. Lett.* **1996**, *256*, 454–464. (b) Stratman, R. E.; Scuseria, G. E.; Frisch, M. J. *J. Chem. Phys.* **1998**, *109*, 8218–8224.

(15) Andrae, D.; Haeussermann, U.; Dolg, M.; Stoll, H.; Preuss, H. *Theor. Chim. Acta* **1990**, *77*, 123–141.

(16) (a) Casida, M. K.; Jamorski, C.; Casida, K. C.; Salahub, D. R. *J. Chem. Phys.* **1998**, *108*, 4439–4449. (b) Stratmann, R. E.; Scuseria, G. E. J. *Chem. Phys.* **1998**, *109*, 8218–8224.

(17) Frisch, M. J.; Trucks, G. W.; Schlegel, H. B.; Scuseria, G. E.; Robb, M. A.; Cheeseman, J. R.; Montgomery, J. A., Jr.; Vreven, T.; Kudin, K. N.; Burant, J. C.; Millam, J. M.; Iyengar, S. S.; Tomasi, J.; Barone, V.; Mennucci, B.; Cossi, M.; Scalmani, G.; Rega, N.; Petersson, G. A.; Nakatsuji, H.; Hada, M.; Ehara, M.; Toyota, K.; Fukuda, R.; Hasegawa, J.; Ishida, M.; Nakajima, T.; Honda, Y.; Kitao, O.; Nakai, H.; Klene, M.; Li, X.; Knox, J. E.; Hratchian, H. P.; Cross, J. B.; Adamo, C.; Jaramillo, J.; Gomperts, R.; Stratmann, R. E.; Yazyev, O.; Austin, A. J.; Cammi, R.; Pomelli, C.; Ochterski, J. W.; Ayala, P. Y.; Morokuma, K.; Voth, G. A.; Salvador, P.; Dannenberg, J. J.; Zakrzewski, V. G.; Dapprich, S.; Daniels, A. D.; Strain, M. C.; Farkas, O.; Malick, D. K.; Rabuck, A. D.; Raghavachari, K.; Foresman, J. B.; Ortiz, J. V.; Cui, Q.; Baboul, A. G.; Clifford, S.; Cioslowski, J.; Stefanov, B. B.; Liu, G.; Liashenko, A.; Piskorz, P.; Komaromi, I.; Martin, R. L.; Fox, D. J.; Keith, T.; Al-Laham, M. A.; Peng, C. Y.; Nanayakkara, A.; Challacombe, M.; Gill, P. M. W.; Johnson, B.; Chen, W.; Wong, M. W.; Gonzalez, C.; Pople, J. A. *Gaussian 03, revision C.02*, Gaussian, Inc.: Wallingford, CT, 2004.

(18) (a) Gorelsky, S. I. *AOMix: Program for Molecular Orbital Analysis*; York University: Toronto, 1997, http://www.sg-chem.net. (b) Gorelsky, S. I.; Lever, A. B. P. *J. Organomet. Chem.* **2001**, *635*, 187–196.

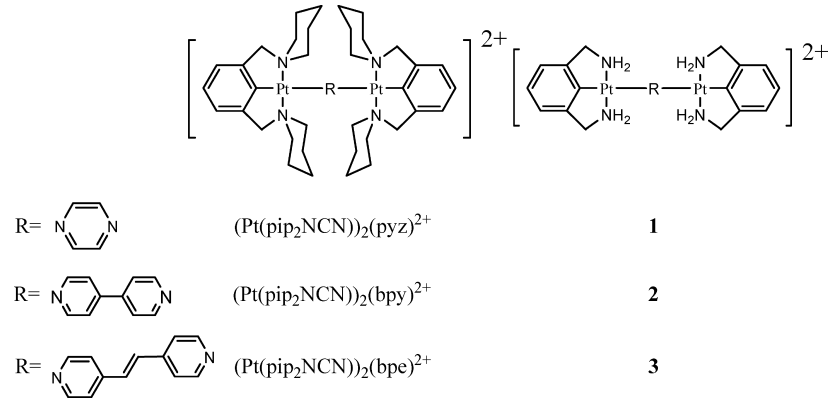

Figure 1. The real systems and their corresponding model systems **1**, **2**, and **3**.

Table 1. Calculated and Experimental (in parentheses)[a] Coordination Bond Lengths (Å) for Models **1**−**3**

	$(Pt(pip_2NCN))_2(pyz)^{2+}$	**1**[b]	**2**[c]	**3**[d]
$Pt-N_{bridge}$	2.189	2.199(2.138)	2.198(2.137)	2.192(2.164)
Pt−C	1.963	1.969(1.936)	1.966(1.927)	1.966(1.910)
$Pt-N_{terminal}$	2.149	2.112(2.104)	2.109(2.103)	2.108(2.097)
				2.109(2.131)

[a] The experimental parameters originate from ref 5. [b] The experimental parameters of **1** originate from crystals of $[Pt(pip_2NCN))_2(\mu\text{-pyz})](CF_3SO_3)_2$ grown by slow evaporation of a CH_2Cl_2/ $CHCl_3$. [c] The experimental parameters of **2** derive from crystals of $[Pt(pip_2NCN))_2(\mu\text{-bpy})]$ $(CF_3SO_3)_2 \cdot {}^1/_2(CH_3)_2CO$ grown by slow evaporation of an acetone−hexanes solution. [d] The experimental parameters of **3** result from crystals of $[Pt(pip_2NCN))_2(\mu\text{-bpe})](CF_3SO_3)_2 \cdot 2CH_2Cl_2$ grown by slow evaporation of CH_2Cl_2/hexanes/Et_2O.

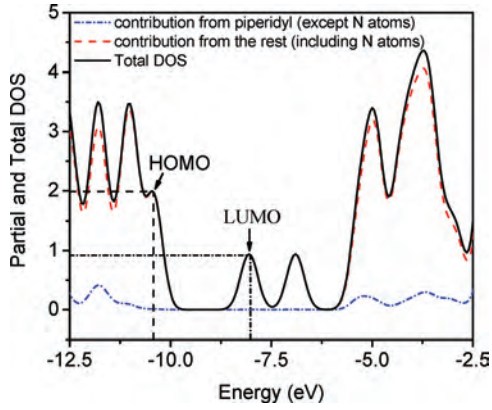

Figure 2. Density-of-states spectrum between the energies of the highest tenth occupied and the lowest tenth virtual orbitals of the complex $(Pt(pip_2NCN))_2(pyz)^{2+}$.

equilibrium geometry. Figure 2 shows the DOS spectra of $[Pt(pip_2NCN)]_2(pyz)^{2+}$ in the energy range from −12.5 to –2.5 eV. This range covers the energies of 20 molecular orbitals (MO) from HOMO-9 to LUMO+9. It was observed that the piperidyls group (except N atoms) contributed little to the total DOS; i.e., replacing this group by NH_2 has no influence on the DOS of complexes. As we all know, the optoelectronic properties of complexes are mainly dependent on their frontier molecular orbitals (FMO). So we could truly study the optoelectronic properties of three platinum(II) dimers using the NH_2 group to replace piperidyl in their structures. The models **1**, **2**, and **3** were thus used throughout our calculations.

3.2. Optimized Molecular Geometries in Ground States. In gas phase, the models **1**, **2**, **3** are in D_2, D_2, and C_i symmetry, respectively. In all cases, the center platinum(II) adopts a distorted square-planar coordination geometry. The dihedral angle between phenyl and bridging ligands for every molecule is close to 80°, and the angle between two pyridyls of bridging ligand for the model **2** is about 43°.

The calculated coordination bond lengths and corresponding experimental values for the models **1**, **2**, **3** are summarized in Table 1. According to the calculation results, the variation of bridging ligands had little effect on the coordination bond lengths, which was a little different from the experimental results. Two factors might account for these differences: First, the experimental crystal parameters were obtained in the presence of the counterion $CF_3SO_3^-$,[5] which may have effect on the molecular geometries.[19] But our calculation system did not consider the potential effect of the counterion. Second, the parameters of three experimental crystals corresponding to the models **1**, **2**, and **3** were obtained in the presence of different solvents.[5] The solvents have a little effect on the structure as well.[20] However, our calculation results for the three models were obtained in gas phase without any solvent effect.

3.3. Electronic Structure. Since the chemical and physical properties of complexes are primarily dependent on their ground-state electronic structures, we focus on the investigation of these electronic structures of the three complexes, especially the frontier orbital components and HOMO–LUMO energy gaps.

The symbols of MOs were assigned on the basis of their compositions, and expressed as s,p(Pt), d(Pt), phenyl ligands (L_{phenyl}), bridging ligand (L_{bridge}) and NH_2, respectively. The energies and compositions of 10 MOs from HOMO-4 to LUMO+4 for the models **1**, **2**, and **3** are plotted in Figure 3 (left). More data are shown in Table S1 in the Supporting Information. Meanwhile, several representative three-dimensional MO plots of the model **1** are also shown in this figure (right). Figure 3 and Table S1 show that the occupied

(19) (a) Fraile, J. M.; Garca, J. I.; Gil, M. J.; Martnez-Merino, V.; Mayoral, J. A.; Salvatella, L. *Chem. Eur. J.* **2004**, *10*, 758–765. (b) Ebrahimi, A.; Habibi, M.; Amirmijani, A. *J. Mol. Struct.-THEOCHEM* **2007**, *809*, 115–124.

(20) (a) Remko, M.; Swart, M.; Bickelhaupt, F. M. *J. Phys. Chem. B* **2007**, *111*, 2313–2321. (b) Ma, W.-Y.; Zhu, Y.-F.; Zhou, J.-H.; Fang, Y.-Z. *J. Mol. Struct.-THEOCHEM* **2007**, *817*, 77–81.

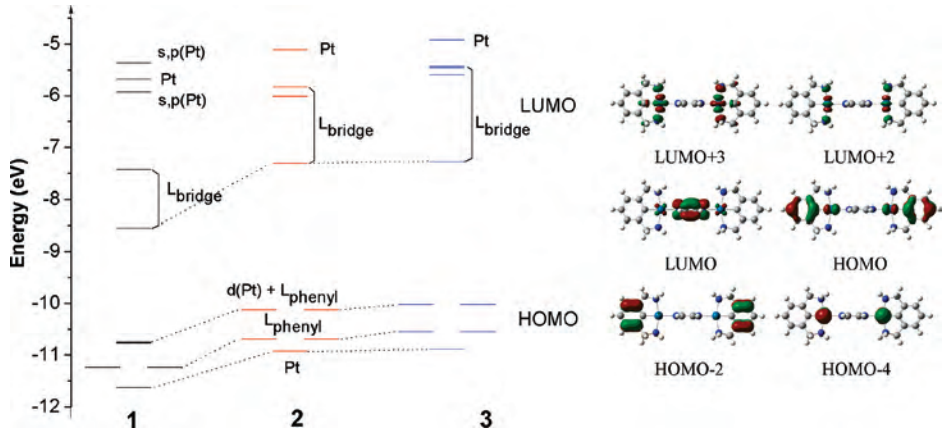

Figure 3. Energy level diagram of frontier molecular orbitals of models **1**−**3** together with representative three-dimensional MO plots of model **1**. (Labels on the right denote the dominant moiety contributing to each molecular orbital.)

orbital compositions, the relative ordering, and characters of the three complexes are almost not influenced by different bridging ligands. The HOMO and HOMO-1 of both **2** and **3** are degenerate orbitals, whereas those of **1** are quasi-degenerate orbitals. These orbitals are mainly delocalized on L_{phenyl} and d(Pt). The HOMO-2 and HOMO-3 of the models **1**, **2**, and **3** are degenerate $\pi(L_{phenyl})$ orbitals, while the HOMO-4 are primarily localized on the center Pt(II). It was observed that some characters of virtual orbitals of **1** are different from those of **2** and **3**. The LUMO+2 and LUMO+3 of **1** are no longer the $\pi^*(L_{phenyl})$ orbitals. Instead, they are Pt(II)-localized orbitals. For the LUMO+4, as the π-conjugated length of bridging ligand increases, the contribution from d(Pt) increases whereas the contribution from s(Pt) and p(Pt) decreases. For this kind of dimer, the HOMOs and LUMOs are located at different coordinated ligands, so it is easy to tune the emission colors of these optoelectronic materials by grafting various electron-withdrawing or electron-donating substituents onto different ligands.

In comparison with model **1**, as the π-conjugated length of bridging ligand increases, the energies of LUMOs and HOMOs of **2** and **3** increase, but the increases in the energies of LUMOs are larger than those of HOMOs. So the energy gaps of **2** (2.82 eV) and **3** (2.74 eV) are higher than that of **1** (2.2 eV). The smallest energy gap of **1** may account for its chemical instability. Although the energy gap of **3** is close to that of **2**, the spectral characters of these two models are different. These points will be further demonstrated in the following sections.

3.4. Bonding Energy. We employed the counterpoise method to evaluate the bonding energy (D_e) of fragments (*NCN*)Pt and $N_{(Lbridge)}$Pt(*NCN*), which was corrected for the basis set superposition error (BSSE).[21] If the fragments (*NCN*)Pt and $N_{(Lbridge)}$Pt(*NCN*) are represented by A and B, respectively, the D_e can be calculated as follows

$$D_e = \Delta E + \mathrm{BSSE}$$

$$\Delta E = E_{AB}^{\{AB\}}(AB) - E_A^{\{A\}}(A) - E_B^{\{B\}}(B)$$

$$\mathrm{BSSE} = E_{AB}^{\{A\}}(A) + E_{AB}^{\{B\}}(B) - E_{AB}^{\{AB\}}(A) - E_{AB}^{\{AB\}}(B)$$

where $E_{AB}^{\{AB\}}(AB)$ is the energy of the optimized AB dimer, $E_A^{\{A\}}(A)$ and $E_B^{\{B\}}(B)$ are the energies of the optimized monomers A and B at their equilibrium geometries, $E_{AB}^{\{A\}}(A)$ and $E_{AB}^{\{B\}}(B)$ are the energies of the components A and B at their own geometries found in the AB dimer, and $E_{AB}^{\{AB\}}(A)$ and $E_{AB}^{\{AB\}}(B)$ are the energies of the components A and B at geometries found in the dimer calculated with the full basis of the dimer {AB}.

D_e can be used to evaluate the stabilities of organometallic complexes. The larger the absolute value of D_e is, the more stable the complex is. For the Pt(II) dimers, as the π-conjugated length of L_{bridge} increases, the calculated D_e increases (3.062, 21.703, and 27.970 kcal/mol for the models **1**, **2**, and **3**). These results indicate that model **1** is not stable as compared with **2** and **3**; i.e., the bond Pt−N_{bridge} of **1** is relatively easy to break. The partial dissociation of $[Pt(pip_2\text{-}NCN)]_2(pyz)^{2+}$ to form the corresponding monomer has been observed in the experiment,[5] which is coincident with our theoretical calculations.

3.5. Reorganization Energy and Ionization Potential. At the microscopic level, the charge transport mechanism can be described as a self-exchange transfer process, in which an electron (or a hole) transfers from a charged molecule to an adjacent neutral molecule.[22] The rate of intermolecular charge transfer (K_{et}) can be estimated by using the semiclassical Marcus theory[23] described as follows

$$K_{et} = A \exp(-\lambda/4K_B T) \qquad (1)$$

where T is the temperature, A is a prefactor related to the electronic coupling between adjacent molecules, λ is the reorganization energy, and K_B is the Boltzmann constant. From eq 1, it can be concluded that the reorganization energy is dominant in the charge transport process at constant temperature; i.e., the overall carrier transfer rates of different molecular structures are mainly dependent on their reorga-

(21) (a) van Duijneveldt, F. B.; van Duijneveldt-van de Rijdt, J. C. M.; van Lenthe, J. H. *Chem. Rev.* **1994**, *94*, 1873–1885. (b) Boys, S. F.; Bernardi, F. *Mol. Phys.* **1970**, *19*, 553–566.
(22) (a) Epstein, A. J.; Lee, W. P.; Prigodin, V. N. *Synth. Met.* **2001**, *117*, 9–13. (b) Reedijk, J. A.; Martens, H. C. F.; van Bohemen, S. M. C.; Hilt, O.; Brom, H. B.; Michels, M. A. J. *Synth. Met.* **1999**, *101*, 475–476. (c) Mott, N. F.; Davis, E. A. *Electronic Processes in Non-Crystalline Materials*, 2nd ed.; Oxford University Press: Oxford, 1979. (d) Geoffrey R., Hutchison; Mark A., Ratner; Tobin J., Marks. *J. Am. Chem. Soc.* **2005**, *127*, 2339–2350.
(23) (a) Marcus, R. A. *J. Chem. Phys.* **1965**, *24*, 966–978. (b) Marcus, R. A. *Rev. Mod. Phys.* **1993**, *65*, 599–610.

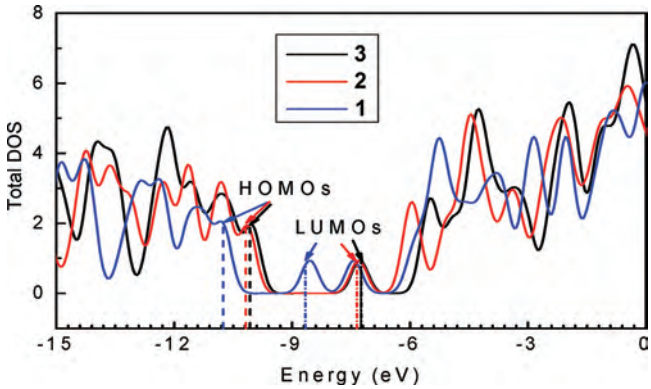

Figure 4. Total density-of-states of models **1**−**3**.

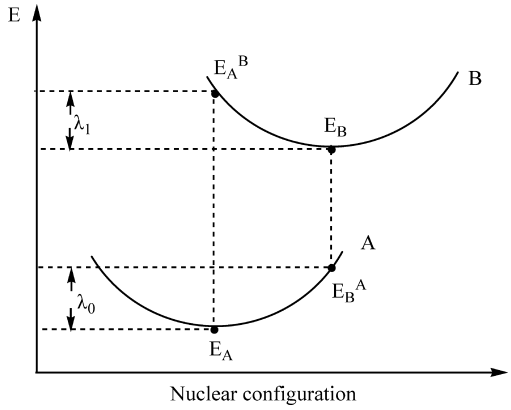

Figure 5. Schematic description of inner reorganization energy calculation.

Table 2. Ionization Potentials and Inner Reorganization Energies for Each Molecule (in eV)

	IP(v)	IP(a)	$\lambda_{i(h)}$	$\lambda_{i(e)}$
1	11.94	11.87	0.19	0.46
2	11.24	11.14	0.16	0.78
3	10.96	10.88	0.25	0.52

nization energies. The low reorganization energy is very necessary to an efficient charge transport process.

Generally, the λ value is determined by fast changes in molecular geometry (the inner reorganization energy λ_i) and slow variations in solvent polarization of the surrounding medium (the external contribution λ_e). In the case of solid-state optoelectronic devices such as LEDs, however, the latter (λ_e) is negligible, thus the λ_i value is approximate to the λ. The inner reorganization energy λ_i is caused by the change of the internal nuclear coordinates from the reactant A to the product B (Figure 5). It can be evaluated as the total of two relaxation energies

$$\lambda_i = \lambda_0 + \lambda_I = (E_A - E_B) + (E_B - E_A) \qquad (2)$$

where E_A and E_B are the energies of A and B at their equilibrium geometries calculated in their own bases {A} and {B}; E_B^A and E_A^B are the energies of A and B at geometries found in the equilibrium geometries of B and A.

The reorganization energies (λ) of the models **1**, **2**, and **3** calculated at the B3LYP/E60 level are listed in Table 2. For each molecule, the reorganization energies for hole transport ($\lambda_{i(h)}$) are smaller than the reorganization energies for electron transport ($\lambda_{i(e)}$). Furthermore, in comparison with the well-known hole-transport material 4,4′-bis(phenyl-m-tolylamino)biphenyl (TPD) ($\lambda_{i(h)}$ = 0.274 eV, $\lambda_{i(e)}$ = 0.689 eV at B3LYP/3-21G* level),[24] these platinum complexes all have relatively small $\lambda_{i(h)}$ (0.16–0.25 eV). These results reveal the hole-transporting performance of these dimers is better than the electron-transporting performance.

In general, the higher the DOS of HOMO or LUMO is, the larger the ability to accommodate holes or electrons is.[25] Figure 4 shows that, for the models **1**, **2**, and **3**, DOS at the energy of HOMO is 2.003, 1.945, and 1.936, while that at the energy of LUMO are 0.939, 0.935, and 0.933. Obviously, these molecules have higher DOS on HOMOs than on LUMOs, indicating that these systems can accommodate more holes in HOMOs and fewer electrons in LUMOs.[25] Accordingly, we further confirm that these Pt(II) dimers favor not electron transport but hole transport.

Ionization potentials (IPs) are also calculated to evaluate the energy barrier for the injection of holes. A low IP means that the holes are easy to inject into devices from the anode, thus the turn-on voltage is low and the performance of devices is good. In contrast to the energy sequence of HOMOs (**1** < **2** < **3**), both vertical IP (IP(v)) and adiabatic IP (IP(a)) decrease (**2** >**3**) as the π-conjugated length of L_{bridge} increases (Table 2). Figure 6 shows the unpaired spin density of **1** mainly distributes on the Pt and L_{phenyl}, which is consistent with the orbital character of the HOMO. These results are true of the other two models. Thus, we assume that the IPs may be decreased by altering the identity of the metal center or introducing electron-releasing substituent into the L_{phenyl}, and the lower energy barrier for the injection of holes is obtained.

3.6. Photoexcitation. To observe the effect of bridging ligand and solvents on the excited-state properties of platinum(II) dimers, TD-B3LYP calculations were performed to evaluate the excitation energies on the basis of the ground-state equilibrium geometries. The effect of solvents was simulated by using the polarizable continuum model included in the GAUSSIAN 03 program. For the selected excited states of the three model systems, the excitation energies calculated in gas phase and CH_2Cl_2 are listed in Table 3 and Table 4, respectively.

An experimentally used model of an excited state corresponds to the excitation of an electron from an occupied MO to a virtual MO (i.e., a one-electron picture). However, the excited states calculated herein demonstrate that excited-state electronic structures had better be described in terms of multiconfiguration, in which a linear combination of several occupied-to-virtual MO excitations comprises a given optical transition. The character of each excited state was assigned on the basis of the compositions of the occupied and virtual MOs of the dominant configuration(s). The excited states originating from transitions between orbitals located on different moieties were classified as charge transfer (CT) excited states such as ligand-to-metal charge transfer (LMCT),

(24) Lin, B. C.; Cheng, C. P.; Lao, Z. P. M. *J. Phys. Chem. A* **2003**, *107*, 5241–5251.
(25) Chu, T.-Y.; Ho, M.-H.; Chen, J.-F.; Chen, C. H. *Chem. Phys. Lett.* **2005**, *415*, 137–140.

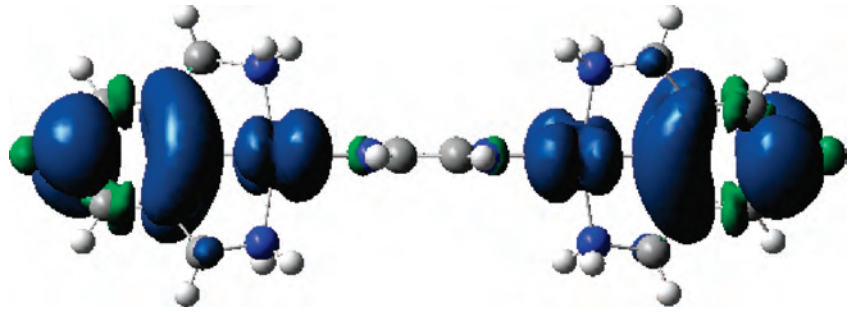

Figure 6. Spin density map of the hole creation for **1**.

Table 3. Selected Excitation Energies (eV), Wavelengths (nm), Oscillator Strenghs (*f*), and Nature for Low-Lying Singlet (S_n) States of Models **1**−**3** Calculated in a Vacuum[a]

	calcd (nm/eV)	state	composition	*f*	nature	λ_{expt} (nm)[b]
1	747.55/1.659	S_1	H → L (0.70)	0.001	MLCT/LLCT	
	374.51/3.311	S_{11}	H-8 → L (0.67)	0.499	MLCT	368/315
		S_{33}	H → L + 4 (0.46)	0.227	MC/LMCT/IL	258
			H-1 → L + 6 (0.38)		MC/LMCT/IL	
2	528.35/2.347	S_1	H → L (0.70)	0.006	MLCT/LLCT	
	329.55/3.762	S_{11}	H-8 → L (0.68)	0.626	MLCT	305/291
	259.31/4.781	S_{39}	H-1 → L + 6 (0.44)	0.204	MC/LMCT/IL	260/277
3	577.97/2.145	S_1	H → L (0.70)	0.005	MLCT/LLCT	
	363.00/3.416	S_7	H-6 → L (0.62)	1.087	IL/MLCT	320
	281.90/4.398	S_{25}	H-12 → L (0.61)	0.690	IL/MLCT	

[a] H denotes HOMO and L denotes LUMO. [b] From ref 5.

Table 4. Selected Excitation Energies (eV), Wavelengths (nm), Oscillator Strenghs (*f*), and Nature for Low-Lying Singlet (S_n) States of Models **1**−**3** Calculated in CH_2Cl_2[a]

	calcd (nm/eV)	state	compositioin	*f*	nature	λ_{expt} (nm)[b]
1	505.47/2.453	S_1	H → L (0.70)	0.000	MLCT/LLCT	
	343.54/3.609	S_9	H-8 → L (0.68)	0.588	MLCT	368/315
	249.44/4.971	S_{30}	H → L + 4 (0.50)	0.435	MC/LMCT/IL	258
			H-1 → L + 5 (0.44)		MC/LMCT/IL	
2	409.74/3.026	S_1	H → L (0.65)	0.002	MLCT/LLCT	
	309.69/4.004	S_7	H-6 → L (0.68)	0.806	MLCT	305/291
	251.96/4.921	S_{27}	H-1 → L + 6 (0.37)	0.480	MC/LMCT/IL	260/277
3	453.06/2.737	S_1	H → L (0.70)	0.005	MLCT/LLCT	
	353.82/3.504	S_7	H-6 → L (0.52)	0.951	IL/MLCT	320
	283.66/4.371	S_{11}	H-10 → L (0.50)		IL/MLCT	
			H-1 → L + 1 (0.44)		MLCT/LLCT	

[a] H denotes HOMO and L denotes LUMO. [b] From ref 5.

metal-to-ligand charge transfer (MLCT), and ligand-to-ligand charge transfer (LLCT). The excited states from π-occupied to π-virtual orbitals located on the same ligand were described as intraligand (IL), and those form orbitals residing on the same metal center were defined as metal centered (MC).

Table 3 and Table 4 show that, whether we consider the solvent effect or not, the lowest transition energies follow the order: **2** > **3** > **1**, which is consistent with the variation rules of the energy gaps because the HOMO → LUMO transition (the coefficient in the configuration interaction wave functions is up to 0.70) is predominant in $S_0 \rightarrow S_1$ electronic transition. Moreover, the lowest excited states are characterized as MLCT[d_{xz}(Pt) → $\pi^*(L_{bridge})$]/LLCT[$\pi(L_{phenyl})$ → $\pi^*(L_{bridge})$]. There is an obvious blue shift in this energy state in solutions as compared with that in gas phase, e.g., the model **1** has an absorption at 1.659 eV in the gas phase whereas the corresponding absorption appears at 2.453 eV in CH_2Cl_2. Overall, the solvent has a significant effect on the transition energies of excited states with the character of MLCT [d(Pt) → $\pi^*(L_{bridge})$]/LLCT [$\pi(L_{phenyl})$ → $\pi^*(L_{bridge})$] (i.e., the first excited states) because such charge transfer makes the electronic density concentrated in the center of the molecules in excited states. Thus, in comparison with the excited states, the ground states are relatively easy to be polarized and stabilized by the polar solvent (CH_2Cl_2), resulting in an obvious blue shift in the spectra.

For the model **1** and **2**, the excited states with the largest oscillator strength are assigned as MLCT[d_{xy}(Pt) → $\pi^*(L_{bridge})$], which are mainly composed of transition from HOMO-8 to LUMO. As the π-conjugated length of L_{bridge} increases, the most intense absorption of **3** is primarily associated with transition from HOMO-6 to LUMO and characterized as IL[$\pi(L_{bridge}) \rightarrow \pi^*(L_{bridge})$] that is mixed with a little of MLCT[d_{xy}(Pt) → $\pi^*(L_{bridge})$]. Moreover, the largest oscillator strengths increase with the π-conjugated length. The solvent effect results in a little blue shift in the most intense absorption.

The second intense absorption bands of **1** and **2** are almost located at the same wavelength with or without solvent effect due to the same transition MC[d_{xz}(Pt) → s,p(Pt)]/LMCT [$\pi(L_{phenyl})$ → s,p(Pt)]/IL[$\pi(L_{phenyl}) \rightarrow \pi^*(L_{phenyl})$], in which the orbitals including the component of L_{bridge} do not participate. The solvent effect just makes these bands blue-shift about 0.181 eV, but it enlarges the oscillator strengths

Table 5. Calculated Excitation Energies of T_1 and Their Transition Nature for Models **1**−**3** at the TD-B3LYP/E60//UB3LYP/E60 Level

	TD-DFT calcd (eV)	composition	*f*	state	nature
1	1.217	L → H (0.73)	0.000	T_1	LMCT/LLCT
2	1.572	L → H (0.70)	0.000	T_1	LMCT/LLCT
3	1.313	L → H-6 (0.63)	0.000	T_1	IL/LMCT
		L → H (0.51)			LMCT/LLCT

approximately two times (more details see the Supporting Information). As the π-conjugated length of L_{bridge} increases, the second intense absorption band of **3** is assigned as IL[$\pi(L_{bridge}) \rightarrow \pi^*(L_{bridge})$], which is mixed with a little of MLCT[$d_{xy}(Pt) \rightarrow \pi^*(L_{bridge})$]. The solvent effect makes the oscillator strength decreased.

It should be pointed out that, although the calculated coordination bond lengths for the models **1**, **2**, **3** deviate from the experimental values a little, especially with respect to the Pt−N_{bridge} bond, they have negligible influence on the spectral properties (see the Supporting Information). In a sense, the experimental absorption spectra can be truly reproduced by theoretical calculations.

3.7. Lowest Triplet Excited States. To gain the correct trend in the evaluation of the Stokes shifts, unrestricted B3LYP was used to optimize the geometries of excited states. The TD-DFT and Δ*S*CF methods were employed to calculate the energies of the lowest triplet excited states (T_1). The former method provides vertical transition energies from the equilibrium geometry of T_1 that is described at the restricted level. The latter estimates the energy of the 0–0 transition, which is the difference between the total energies of the structures optimized in the ground state and those in the triplet excited state. In contrast to the TD-DFT formalism described above, the Δ*S*CF approach treats the triplet excited states as the excitation of an electron from an occupied MO to a virtual MO (i.e., a one-electron picture).

The calculation results show that the axial metal–ligand bond lengths in excited states are shorter than those in ground states. For example, (Pt−N_{bridge}, Pt−C) of **1** in the lowest triplet and ground states are (2.132, 1.947 Å) and (2.199, 1.969 Å), respectively. The dihedral angles between phenyl and bridging ligands of **1** and **3** are reduced to 54.1° and 47.0°, whereas that of **2** is increased to 87.2°. The bridging ligand of **2** is no longer distorted, instead, it tends to be complanate in triplet state.

The results of the TD-DFT calculations are summarized in Table 5. Meanwhile, a graphical display for the changes of electron density distribution upon $T_1 \rightarrow S_0$ excitation is shown in Figure 7. Similar to the energy gaps of ground states, the triplet excitation energies follow the order: **2** > **3** > **1** (see Table 5). Figure 7 shows that the characters of triplet excited states gradually change with the π-conjugated length of L_{bridge}. The triplet states of **1** and **2** are dominated by L → H transitions, which can be assigned as LMCT[$\pi^*(L_{bridge}) \rightarrow d_{xz}(Pt)$]/LLCT[$\pi^*(L_{bridge}) \rightarrow \pi(L_{phenyl})$]. T_1 of **3** is described by the L → H-6 and L → H excitations, mainly corresponding to IL[$\pi^*(L_{bridge}) \rightarrow \pi(L_{bridge})$]/LMCT[$\pi^*(L_{bridge}) \rightarrow d_{xy}(Pt)$ or $d_{xz}(Pt)$]/LLCT [$\pi^*(L_{bridge}) \rightarrow \pi(L_{phenyl})$].

In addition, the nature of T_1 was also analyzed by the ΔSCF method. Table 6 lists the subtractive value between net Mulliken charge distribution of the lowest triplet state and that of the ground state, together with the sum of Mulliken atomic spin densities of the lowest triplet state over different fragments. The spin density distribution provided by unrestricted DFT calculations can clearly explain the localization of the triplet wave function. For the models **1** and **2**, Mulliken spin densities of T_1 mainly delocalize in Pt, L_{phenyl}, and L_{bridge}, and the sum of Mulliken spin densities of Pt and L_{phenyl} is equal to that of L_{bridge}. Considering the variation of Mulliken charge over different fragments, it can be concluded that the distribution of Mulliken spin densities of T_1 originates from the transfer of the net Mulliken charges from Pt and L_{phenyl} to L_{bridge}. Hence, when electrons transfer from the lowest triplet excited state to the ground state, the corresponding spectral characters of **1** and **2** are assigned as LMCT[$\pi^*(L_{bridge}) \rightarrow d_{xz}(Pt)$]/ LLCT[$\pi^*(L_{bridge}) \rightarrow \pi(L_{phenyl})$], which is coincident with the description of TD-DFT method. In contrast to **1** and **2**, the model **3** transfers very few net Mulliken charges ($0.218e^-$). The sum of Mulliken spin densities of Pt and L_{phenyl} is much smaller than that of L_{bridge}, and thus Mulliken spin densities of T_1 are governed by L_{bridge} fragment. Accordingly, the spectral nature of **3** is reasonably characterized as IL[$\pi^*(L_{bridge}) \rightarrow \pi(L_{bridge})$], which agrees well with the experiment. However, it is a little different from the depiction of the TD-DFT method. The difference between the calculated results of the two methods is mainly attributed to the tendency of the triplet wavefuction to get localized in the spin-unrestricted calculations, which benefit locally excited configurations and thus reduce the MLCT and LLCT contributions.[26]

It should be pointed out that, in experiments,[5] the bpy dimer exhibits structural emission from a lowest pyridyl-centered $^3(\pi \rightarrow \pi^*)$ excited state. However, the calculated results of TD-DFT and ΔSCF methods do not agree with the experimental results. The calculated emission energies, especially for the results calculated by the TD-DFT method, do not agree well with the experimental data. They may be attributed to the limitations of the computational methods. It is well-known that the TD-DFT method can yield substantial errors for valence excited states of molecules exhibiting a spatially extended π-system and for charge-transfer excited states.[27] Although we have used the HF/DFT hybrid functional B3LYP that can partially overcome the asymptotic problem, the correct $1/R$ (R is the distance

(26) (a) Avilov, I.; Minoofar, P.; Cornil, J.; Cola, L. D. *J. Am. Chem. Soc.* **2007**, *129*, 8247–8258. (b) Beljonne, D.; Cornil, J.; Brédas, J. L.; Friend, R. H.; Janssen, R. A. J. *J. Am. Chem. Soc.* **1996**, *118*, 6453–6461. (c) Beljonne, D.; Cornil, J.; Brédas, J. L.; Friend, R. H. *Synth. Met.* **1996**, *76*, 61–65. (d) Beljonne, D.; Wittmann, H. F.; Köhler, A.; Graham, S.; Younus, M.; Lewis, J.; Raithby, P. R.; Khan, M. S.; Friend, R. H.; Brédas, J. L. J. *Chem. Phys.* **1996**, *105*, 3868–3877. (e) Dos Santos, D. A.; Beljonne, D.; Cornil, J.; Brédas, J. L. *Chem. Phys.* **1998**, *227*, 1–10. (f) Avilov, I.; Marsal, P.; Brédas, J. L.; Beljonne, D. *Adv. Mater.* **2004**, *16*, 1624–1629.

(27) (a) Grimme, S.; Parac, M. *ChemPhysChem* **2003**, *3*, 292–295. (b) Casida, M. E.; Gutierrez, F.; Guan, J.; Gadea, F. X.; Salahub, D.; Daudey, J. P. *J. Chem. Phys.* **2000**, *113*, 7062–7071. (c) Dreuw, A.; Weisman, J. L.; Head-Gordon, M. *J. Chem. Phys.* **2003**, *119*, 2943–2946. (d) Cai, Z. L.; Sendt, K.; Reimers, J. R. *J. Chem. Phys.* **2002**, *117*, 5543–5549.

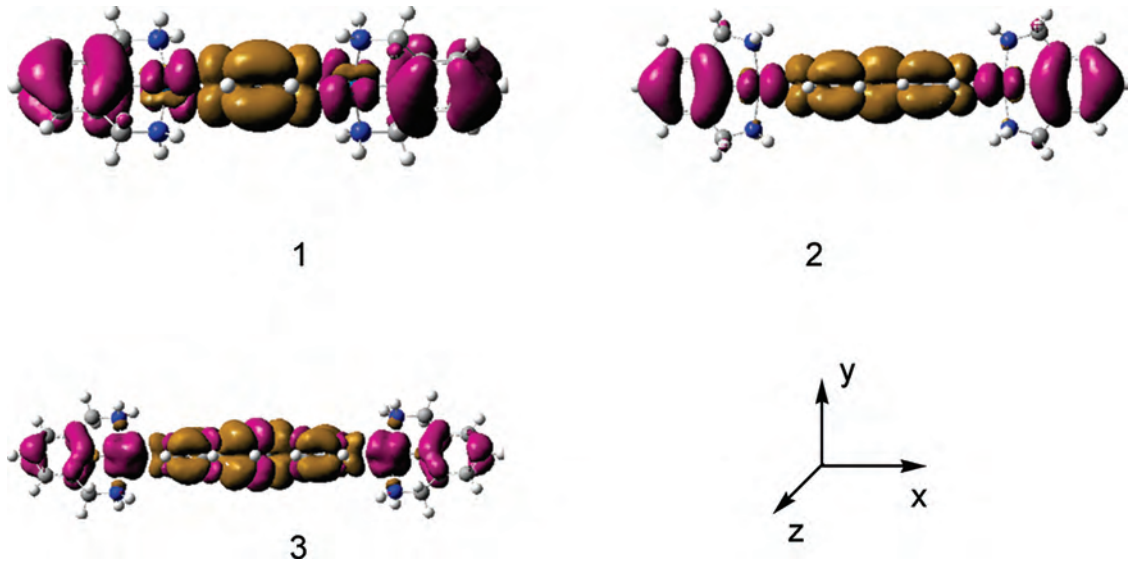

Figure 7. Change of electron density distribution upon the $T_1 \rightarrow S_0$ electronic transition of models **1**−**3**. Yellow and violet colors correspond to a decrease and increase of electron density, respectively.

Table 6. Calculated Excitation Energies of T_1 and Their Transition Nature for Models **1**−**3** at the ΔSCF Level, the Subtractive Value between Net Mulliken Charge Distribution of the Lowest Triplet State and that of the Ground State, and the Sum of Mulliken Atomic Spin Densities of the Lowest Triplet State over Different Fragments

	ΔSCF		Mulliken charge (e^-)				Mulliken spin density (e^-)			
	calcd (eV)	nature	Pt	L_{phenyl}	L_{bridge}	NH_2	Pt	L_{phenyl}	L_{bridge}	NH_2
1	2.093	LMCT/LLCT	0.306	0.200	−0.548	0.043	0.400	0.568	1.029	0.002
2	2.572	LMCT/LLCT	0.283	0.298	−0.646	0.065	0.384	0.613	1.001	0.002
3	1.937	IL	0.125	0.073	−0.218	0.019	0.173	0.133	1.687	0.007

of the electron from the nuclei)[28] asymptotic behavior of CT states cannot be achieved yet. Moreover, the studied systems are put in a gas-phase environment for the quantum method, whereas the emission spectra are measured in solid state, which cannot be considered in our methods.

In addition, the calculated vertical transition energies are much smaller than 0–0 $T_1 \rightarrow S_0$ transition energies, revealing that the geometrical relaxation energies of T_1 are significant, especially for the model **2** (the difference of energy values is 1 eV). The dihedral angle of **2** between two pyridyls of bridging ligand changes from 43° in ground state to 0° in triplet state.

Overall, the electronic structures and spectral characters of excited states of these platinum(II) dimers can be controlled by the π-conjugated length of L_{bridge}. The nature of excited states changes from LLCT/LMCT to IL as the π-conjugated length of L_{bridge} increases. Furthermore, we can also alter the luminescent wavelength by modifying phenyl and bridging ligands.

3.8. Third-Order Polarizability. Our calculation results reveal the studied systems possess donor–acceptor–donor (D−A−D) configurations, and they should have larger intramolecular charge transfer under the external electronic field. Moreover, in view of the energy of the UV–vis spectrum, these complexes satisfy high transparency in the visible light area according to Gomper's research.[29] This transparency is worthy of remarks in terms of practical applications in the nonlinear optical (NLO) field. We anticipate that these complexes offer some new interesting opportunities to third-order NLO materials. The third-order polarizabilty (γ) was calculated by using TD-DFT combined with the sum-over-states (SOS) method. First, 60 excited states were calculated using TD-B3LYP model. Those physical values then served as the input of the SOS formula to calculate the third-order polarizability. Our group has used this method to investigate the NLO properties of a series of compounds.[30] Specific calculation information can be seen in the ref.[30d]

An average γ is obtained from the formula $\gamma = 1/5(\gamma_{xxxx} + \gamma_{yyyy} + \gamma_{zzzz} + \gamma_{xxyy} + \gamma_{xxzz} + \gamma_{yyxx} + \gamma_{yyzz} + \gamma_{zzxx} + \gamma_{zzyy})$. The static third-order polarizability is termed the zero-frequency hyperpolarizability and is an estimate of the intrinsic molecular hyperpolarizability in the absence of the resonance effect. The calculated γ for models **1**, **2**, and **3** are -103.2×10^{-36}, -86.8×10^{-36}, and -538.4×10^{-36} esu, respectively. The calculated values are several times higher than those of typical compounds with extensive π-electron conjugation, e.g., the calculated γ value of **3** is about 7 times higher than the average third-order polarizability of the C_{60} molecule[31] and 11 times higher than that

(28) Casida, M. E.; Jamorski, C.; Casida, K. C.; Salahub, D. R. *J. Chem. Phys.* **1998**, *108*, 4439–4449.
(29) Gompper, R.; Mair, H. J.; Polborn, K. *Synthesis* **1997**, *6*, 696–718.
(30) (a) Yang, G. C.; Su, Z. M.; Qin, C. C.; Zhao, Y. H. *J. Chem. Phys.* **2005**, *123*, 134302. (b) Yang, G. C.; Su, Z. M.; Qin, C. C. *J. Phys. Chem. A* **2006**, *110*, 4817–4821. (c) Yang, G. C.; Liao, Y.; Su, Z. M.; Zhang, H. Y.; Wang, Y. *J. Phys. Chem. A* **2006**, *110*, 8758–8762. (d) Yang, G. C.; Guan, W.; Yan, L. *J Phys. Chem. B* **2006**, *110*, 23092–23098.
(31) Wang, Y.; Cheng, L. T. *J. Phys. Chem.* **1992**, *96*, 1530–1532.

measured for highly π-delocalized ruthenium(II) complexes.[32] Thus, we predict that the studied systems, especially model **3**, may have excellent third-order NLO response.

For the SOS method, the third-order polarizability is governed by the product of the transition moments and the transition energy. In general, as the transition moment increases, the third-order polarizability increases, whereas the high transition energy corresponds to the low third-order polarizability. From Table 3, it can be observed that model **3** has the strongest oscillator strength whereas its transition energy is relative low, implying that **3** has the largest transition moment because the oscillator strength is proportional to the transition energy and transition moment ($f = (8\pi^2 m_e/3e^2h)E_{ng}\mu_{ng}^2$). Thus, the largest γ is obtained. The third-order polarizability of **1** is a little larger than that of **2** because of the lower transition energy of MLCT excited state. Moreover, all the systems have negative third-order polarizabilities, as reported previously.[30d] Such all-optical nonlinearities are self-defocusing rather than self-focusing, eliminating the concern of the nonlinear optical autooptical annihilation of a potential all-optical device. In addition, negative γ has been instrumental in helping define the family of microscopic electronic mechanisms.[30d,33]

According to the above analysis, we can conclude that, for this kind of Pt(II) dimer, new optoelectronic materials with the large third-order polarizability could be designed by altering the donors or acceptors, e.g., introducing electron-releasing substituent into peripheral L_{phenyl}, grafting electron-withdrawing substituent (or heteroatom such as N atom) into the central L_{bridge}, or enlarging π-conjugation of L_{bridge}.

4. Conclusion

We have performed a comprehensive study of photophysical properties of three platinum(II) dimers $(Pt(pip_2NCN))_2(L)^{2+}$ (where L represents the bridging ligands pyz, bpy, and bpe), focused on the effect of the π-conjugated length of the bridging ligand. The results indicate that, as the π-conjugated length of bridging ligand increases, the energies of HOMOs and LUMOs, bonding energy of $Pt-N_{bridge}$, and the largest absorption strength increase, whereas the ionization potentials decrease. In terms of inner reorganization energy and density of states, we presume the hole-transporting performance of these dimers is better than the electron-transporting performance, and their inner reorganization energies for hole transport are lower than that of TPD, a widely used hole-transporting material. These complexes, especially $(Pt(pip_2NCN))_2(bpe)^{2+}$, have potential to be excellent third-order nonlinear optical materials, owing to their large third-order polarizabilty value and high transparency.

Our calculation results reveal that, for this kind of dimer, the transition energy of the designed optoelectronic materials can be reduced by introducing electron-releasing substituent into peripheral phenyl ligand, introducing electron-withdrawing substituent (or heteroatom) into the central bridging ligand, or enlarging π-conjugation of bridging ligand. Thus, the energy barrier for the hole injection of the desired materials becomes lower, and their third-order polarizability becomes larger, resulting in an improved performance of devices. Further studies on this aspect are in progress.

Acknowledgment. We are grateful to the grants from the National Natural Science Foundation of China (No. 20373009 and 20573016), the Specialized Research Fund for the Doctoral Program in Higher Education Institutions of the Ministry of Education of China (No.20030183063) for financial support and PCSIRT. Science Foundation for Young Teachers of Northeast Normal University (No.20060311, 20060302, 20060307 and 20061004) is also greatly appreciated.

Supporting Information Available: The energy and the composition of the highest five occupied and lowest five virtual orbitals for models **1**−**3**, the solvent effect on the oscillator strengths of the second intense absorption bands of models **1** and **2**, and the effect of $Pt-N_{bridge}$ bond on the spectral properties. This material is available free of charge via the Internet at http://pubs.acs.org.

IC7018154

(32) Hurst, S. K.; Cifuentes, M. P.; Morrall, J. P. L.; Lucas, N. T.; Whittall, I. R.; Humphrey, M. G.; Asselberghs, I.; Persoons, A.; Samoc, M.; Luther-Davies, B.; Willis, A. C. *Organometallics* **2001**, *20*, 4664–4675.

(33) (a) Dirk, C. W.; Cheng, L.-T.; Kuzyk, M. G. *Int. J. Quantum Chem.* **1992**, *43*, 27–36. (b) Dirk, C. W.; Cheng, L.-T.; Kuzyk, M. G. *Mater. Res. Soc. Symp. Proc.* **1992**, *247*, 73. (c) Gorman, C. B.; Marder, S. R. *Proc. Natl. Acad. Sci. U.S.A.* **1993**, *90*, 11297–11301.